Accepted Manuscript

Kinetics of Gas Phase Formic Acid Decomposition on Platinum Single Crystal and Polycrystalline Surfaces

Michael D. Detwiler, Cory A. Milligan, Dmitry Y. Zemlyanov, W. Nicholas Delgass, Fabio H. Ribeiro

PII: S0039-6028(15)00423-9
DOI: doi: 10.1016/j.susc.2015.12.021
Reference: SUSC 20760

To appear in: *Surface Science*

Received date: 10 October 2015
Revised date: 17 December 2015
Accepted date: 18 December 2015

Please cite this article as: Michael D. Detwiler, Cory A. Milligan, Dmitry Y. Zemlyanov, W. Nicholas Delgass, Fabio H. Ribeiro, Kinetics of Gas Phase Formic Acid Decomposition on Platinum Single Crystal and Polycrystalline Surfaces, *Surface Science* (2015), doi: 10.1016/j.susc.2015.12.021

This is a PDF file of an unedited manuscript that has been accepted for publication. As a service to our customers we are providing this early version of the manuscript. The manuscript will undergo copyediting, typesetting, and review of the resulting proof before it is published in its final form. Please note that during the production process errors may be discovered which could affect the content, and all legal disclaimers that apply to the journal pertain.

ACCEPTED MANUSCRIPT

Kinetics of Gas Phase Formic Acid Decomposition on Platinum Single Crystal and Polycrystalline Surfaces

Michael D. Detwiler,[†] Cory A. Milligan, [†] Dmitry Y. Zemlyanov, [‡] W. Nicholas Delgass,[†] and Fabio H. Ribeiro*,[†]

†School of Chemical Engineering, Purdue University, West Lafayette, Indiana, 47907, United States

‡Birck Nanotechnology Center, Purdue University, West Lafayette, Indiana, 47907, United States

Keywords: Formic Acid Decomposition; Platinum; Structure Sensitivity; Kinetics; Single Crystal; Ultra-high Vacuum

ABSTRACT

Formic acid dehydrogenation turnover rates (TORs) were measured on Pt(111), Pt(100), and polycrystalline Pt foil surfaces at a total pressure of 800 Torr between 413 – 513 K in a batch reactor connected to an ultra-high vacuum (UHV) system. The TORs, apparent activation energies, and reaction orders are not sensitive to the structure of the Pt surface, within the precision of the measurements. CO introduced into the batch reactor depressed the formic acid dehydrogenation TOR and increased the reaction's apparent activation energies on Pt(111) and Pt(100), consistent with behavior predicted by the Temkin equation. Two reaction mechanisms were explored which explain the formic acid decomposition mechanism on Pt, both of which include dissociative adsorption of formic acid, rate limiting formate decomposition, and quasi-equilibrated hydrogen recombination and CO adsorption. No evidence was found that catalytic supports used in previous studies altered the reaction kinetics or mechanism.

ACCEPTED MANUSCRIPT

INTRODUCTION

Conversion of biomass to liquid fuels and valuable chemicals requires a large hydrogen input. Formic acid, a byproduct of many of these upgrading reactions, can catalytically decompose to produce H_2 and CO_2 or H_2O and CO. On Pt, reported dehydrogenation selectivity is near 100% [1, 2]. In this study, the formic acid dehydrogenation kinetics on Pt(111), Pt(100), and a Pt foil were measured at a total pressure of 800 Torr and temperatures between 413 – 513 K. TORs did not vary on the surfaces tested within the precision of the measurements. In this work, we compare the results obtained here to other formic acid decomposition studies on Pt in the literature and discuss simple reaction mechanisms for formic acid dehydrogenation.

METHODS AND MATERIALS

Kinetics were measured in a gas phase 1.4 L stainless steel batch reactor connected to a UHV chamber via a welded metal bellows transfer arm allowing for sample transfer between the two chambers in vacuum. This apparatus has been described previously [3, 4]. The batch reactor was pumped with a turbomolecular pump in order to reach pressures < 1 x 10^{-6} Torr for sample transfer to the UHV chamber. The UHV chamber was equipped with an ion gun (PHI 04-161) and resistive heating of sample, a PHI 15-255G double pass cylindrical mirror electron energy analyzer with a build-in electron gun and a Mg x-ray source for x-ray photoelectron spectroscopy (XPS) and Auger electron spectroscopy (AES), and low energy electron diffraction (LEED) (OCI Vacuum Microengineering BDL800IR-ISH-FIX). The UHV chamber was also equipped with a UTI-100C quadrupole mass spectrometer. The base pressure of the UHV chamber was ~ $5x10^{-10}$ Torr.

Pt Single Crystal and Foil Samples

ACCEPTED MANUSCRIPT

Pt(100) and Pt(111) single crystals (Princeton Scientific) with orientation accuracy < 0.1° were spot welded to the sample holder via stainless steel pins on each side of the crystal. Current was passed directly through the pins for resistive heating. A Eurotherm 2408 temperature controller controlled crystal temperature which was measured by a K-type thermocouple spot welded to the side of the single crystal or back of the foil. Each sample was remounted and the thermocouple leads were re-welded several times during a campaign of kinetic experiments.

Samples were prepared before each series of experiments by repeated cycles of Ar^+ sputtering (5 x 10^{-5} Torr Ar, 1-2 keV electrons), O_2 treatment (1 x 10^{-6} to 2 x 10^{-5} Torr, 773-1073 K), and annealing in vacuum at 1073 K. Samples were checked for contaminants by AES or XPS after cleaning to confirm that no contaminants were present on the sample surface other than C or O, which were unavoidable from residual formic acid vapor and background CO and H_2O. A detailed discussion of sample cleanliness is given in the results section. Single crystal samples were checked by LEED to ensure that the expected surface construction was present. Hexagonal (111)-(1x1) and square (100)-(1x1) diffraction patterns were observed on the Pt(111) and (100) crystals after the standard cleaning procedure, respectively. For Pt(100), as noted, residual contamination lifted the hexagonal reconstruction [5].

Kinetic Experiments and Kinetic Data Analysis

Reaction gases and vapors were introduced to the batch reactor one by one via stop valves on the gas manifold which was pumped by a scroll pump after dosing each gas. An MKS Baratron pressure transducer with ± 0.1 Torr accuracy was used to monitor the amount of gas introduced to the reactor. Formic acid (Thermo Scientific, 99+%) and water (Millipore, 18.2 MΩ resistivity) were introduced from the vapor space in sealed glass containers containing 1-2 mL of the liquid. Each liquid was degassed before reaction by several cycles of freeze-pump-thaw. Other gases

ACCEPTED MANUSCRIPT

used were CO (Research purity, Matheson, 99.998%), H_2 (Praxair, UHP, 99.999%), and N_2 (Research grade, Airgas, 99.9997%). Gas dosing order was typically formic acid, water (if dosed), H_2, CO, and balance N_2 for a total pressure of 800 Torr. For some runs CO was dosed before H_2, but this did not have a measureable impact on the CO_2 turnover rate (TOR). After dosing, gases were circulated in two loops by two bellows pumps (Metal Bellows, MB-21). One circulation loop included a Nicolet Nexus 670 Fourier transform infrared (FTIR) spectrometer with a gas cell for analysis. Gases were permitted to mix for approximately 5 minutes before data collection began to ensure a well-mixed system.

Kinetic Experiments

CO_2 TORs were calculated by measuring the CO_2 evolution monitored by the gas phase asymmetric stretching mode IR peak at 2349 cm^{-1}. A data point from 25 averaged spectra was collected approximately every 10 s using Omnic version 7.2a data acquisition software. CO_2 concentration was related to absorbance using a calibration curve prepared by measuring the CO_2 absorbance peak area for several dilutions of a 500 ± 2% ppm CO_2 in N_2 gas mixture. The batch reactor walls were kept at room temperature during all experiments. Bulk reaction gas temperature change due to heating of the sample in the 140-240 ºC range was negligible, as the formic acid dimer to monomer ratio remained constant during reaction. This was possible because the recirculation flow kept the volume of heated gas near the sample small and the heat added to the gas by the sample was lost through the walls of the reactor and recirculation system.

CO_2 TORs were calculated by numerically differentiating batch reactor data and were normalized to the calculated geometric Pt atom density of the front face of each single crystal: 1.5×10^{15} and 1.3×10^{15} Pt atoms cm^{-2} for Pt(111) and (100), respectively. Pt atom density on the Pt foil surface was assumed to be 1.5×10^{15} cm^{-2}. The backsides of each sample were

ACCEPTED MANUSCRIPT

assumed to be inactive because they were neither polished nor sputter cleaned. Reported TORs were collected following cleaning of the sample and then after at least one run ≥ 30 min. The TOR usually dropped considerably after this first run then remained roughly constant for subsequent runs. A detailed discussion is given in the results section.

Activation energy and reaction order runs were performed multiple times on different days in the stable kinetic regime. For activation energy measurements, temperature was varied over the relevant temperature range dwelling at each point for 2 to 5 minutes. Temperatures were varied randomly, and at least the final point was collected at the same temperature as the first point in order to account for catalyst deactivation and hysteresis. Because reactions were run in batch mode, gases were recharged for each point for an order collection experiment. Concentrations for reaction order experiments were varied randomly and the first point was always repeated at the end of the series to account for catalyst deactivation and hysteresis. Formic acid reaction orders are plotted against the natural log of effective formic acid monomer concentration which takes into account the presence of dimer in the gas phase. The partial pressures of the formic acid monomer, P_m, and dimer, P_d, fractions are expressed in Equation 1:

$$K = \frac{{P_m}^2}{P_d} = 10^{\left(10.755 - \frac{3090}{T}\right)} Torr \qquad (1)$$

where K is the equilibrium constant [6, 7] and T is the temperature in degrees Kelvin. Equation 1 was used to calculate the partial pressures of monomer and dimer present in the gas phase.

Ex situ Characterization

AES spectra were collected using 3 keV incident electrons in differential mode using a PHI lock-in amplifier. XPS spectra were collected using a non-monochromated Mg source (hν = 1253.6 eV) with constant pass energy = 50 eV. The binding energy scale was calibrated using Au

ACCEPTED MANUSCRIPT

$4f_{7/2}$ and Cu $2p_{3/2}$ peaks at 83.8 eV and 932.4 eV, respectively, taken from a sputter cleaned sample containing Au and Cu foils. The fwhm of the Au $4f_{7/2}$ line was 1.36 eV. Spectra were analyzed using CasaXPS version 2.3.16 PR 1.6 (Casa Software Ltd.). To calculate coverage from XPS results, we followed Fadley's approach, [8] which assumes a non-attenuating adlayer at fractional coverage. Coverage (Θ), measured in monolayers (ML), is the ratio between the number of adsorbed species and the number of surface Pt atoms on (111) plane, and is expressed in Equation 2:

$$\Theta = \frac{N_l(\theta)}{\frac{d\sigma_l}{d\Omega}} \times \frac{\frac{d\sigma_s}{d\Omega}}{N_s(\theta)} \times \frac{\text{Instrument Function}(E_s)}{\text{Instrument Function}(E_l)} \times \frac{\Lambda_e^{subst}(E_s)}{d_s} \times cos\theta \qquad (2)$$

where $N_l(\theta)$ and $N_s(\theta)$ are the photoemission peak areas of the adlayer and the substrate at the given photoemission angle, θ, with respect to the surface normal; $\text{Instrument Function}(E_s)$ and (E_l) includes the acceptance solid angles of the electron analyzer and the effective analyzed areas for the photoelectrons from substrate and adlayer; $d\sigma_l/d\Omega$ and $d\sigma_s/d\Omega$ are differential cross-sections for the photoemission peaks of the adlayer and the substrate, which are calculated using tabulated Scofield cross-sections [9] and the Reilman asymmetry parameters; [10] $\Lambda_e^{subst}(E_s)$ is the electron attenuation length (EAL) of the photoelectrons originating from the substrate atom that have traveled through the substrate material; and ds is the interlayer distance of the substrate. The EAL was calculated by NIST SRD-82. [11]

RESULTS

Analysis of the Gas Phase IR Spectra

ACCEPTED MANUSCRIPT

Figures S1 and S2 in the supplementary information show FTIR spectra before and after 52 minutes of reaction on Pt(100) at 473 K respectively. Assignments for formic acid monomer and dimer peaks are given in Table S1 in the supplementary information. The only observed product of formic acid decomposition was CO_2, evident from the increase in absorbance of the asymmetric CO_2 stretching peak at 2349 cm^{-1}. CO and H_2O, dehydration products, were not observed above the limit of detection. CO could not be quantified in any kinetic experiments for which CO was co-fed. For experiments where CO was not co-fed, no intensity change was observed in the C=O stretching region at 2143 cm^{-1}. The limit of detection for CO was about 0.5 ppm. For all experiments, dehydrogenation selectivity was > 99%. Asymmetric stretching features of water between 1400-1700 cm^{-1} were present in background spectra barely above the noise level due to impurity of the formic acid (99+% pure), these were not quantified, and did not change during reaction.

System Validation

To ensure that measured rates resulted from formic acid decomposition on the Pt surface, two blank experiments were performed. In the first, the CO_2 TOR was measured on a piece of 316 stainless steel (SS) foil spot welded between the two heating leads. The areal rate at 493 K on the 316 stainless steel blank was approximately 5 x 10^{-10} moles CO_2 cm^{-2} s^{-1}, while the measured areal rates on Pt(111) and Pt(100) under the same conditions were greater than 6 x 10^{-9} and 8 x 10^{-9} moles CO_2 cm^{-2} s^{-1}, respectively. The areal rate of 5 x 10^{-10} moles CO_2 cm^{-2} s^{-1} represents a maximum rate on surfaces other than the active Pt for a reaction with catalyst present, as the blank was replaced with the actual catalyst, so only decomposition on the stainless steel heating pins would lead to an error in the rate measurement on SS surfaces.

ACCEPTED MANUSCRIPT

In the second validation experiment the background activity of the batch reactor was measured with a Pt catalyst present. With Pt(111) loaded, the reactor was charged with gases used under standard conditions except for formic acid (15 Torr H_2, 15 Torr CO, 800 Torr total, balance N_2). At 493 K, the measured CO_2 formation TOR on Pt(111) was approximately 0.05 molecules CO_2 (Pt atom)$^{-1}$ s^{-1}. Under the same conditions with 5 Torr formic acid present, the average TOR on Pt(111) was 2.6 ± 0.6.

The rate reported throughout this work is the rate of formation of CO_2. Direct calibration and measurement of CO_2 peak area instead of using formic acid peaks (both monomer and dimer contributions) is a more straightforward route for calculation of the decomposition TOR. The formic acid decomposition TOR was measured for comparison to the CO_2 TOR for an experiment with 1 Torr initial pressure of formic acid (P_{H2} = 15 Torr, Total Pressure 800 Torr, balance N_2). The CO_2 TOR calculated for this run at 473 K was 1.80 molecules CO_2 (Pt atom)$^{-1}$ s^{-1}. The decomposition TOR of formic acid was measured to be 1.77 molecules formic acid (Pt atom)$^{-1}$ s^{-1}, calculated by the decrease in the ν(C-O) peaks for monomer and dimer at 1106 and 1218 cm^{-1}, respectively, where concentrations of monomer and dimer were calculated using Equation 1, indicating that the generation of CO_2 can be fully attributed to formic acid decomposition. Additionally, the dehydrogenation rates of the formic acid monomer and ½ dimer for this experiment were both equal to ~0.6 s^{-1} (resulting in the total overall rate of 1.8 s^{-1} reported above by adding 2 times the dimer TOR to the monomer TOR), indicating that formic acid dimers readily decomposed forming two monomers near or on the hot catalytic surface.

Internal heat and mass transfer limitations were not present, as the single crystals and Pt foil were non-porous. Based on the data shown below in Figure 3 and data gathered previously on this system, external heat and mass transfer limitations also do not affect the rate. Smeltz et al.

ACCEPTED MANUSCRIPT

measured a TOR of 0.34 ± 0.02 s^{-1} for NO oxidation on Pt(111) using the same reactor system at 573 K, and verified that the rate of mass transfer to the surface was at least one order of magnitude higher than the rate of reaction using reaction gas mixtures of < 100 ppm for NO and NO_2 [4]. Since the gas concentrations in this study were much higher (with the exception of CO_2) and thus would accentuate diffusion because of the steeper gradient at the surface but the TORs observed at 413 K under the conditions used in Figure 3 on Pt(100) were similar to those for NO oxidation (red line, TOR = 0.37 s^{-1}), we conclude that the external diffusion rate well exceeds the reaction rate. Further evidence is given by the observation that, in the same activation energy run, TORs as high as 3.45 s^{-1} were measured, and all points fell on the same line.

The variability in TOR due to the mounting position of the thermocouple on the Pt single crystals was found to be much less than the day-to-day variability in measured TOR, as the TOR at standard conditions and other kinetic parameters (activation energy, reaction orders) were collected several times over the course of several months during which time the sample was remounted many times.

Rate Stabilization

Supported catalysts in flow reactors are typically subjected to long stabilization periods under reaction conditions before kinetic measurements begin. This approach is not possible for batch reactors. Therefore, the TOR was permitted to stabilize during several consecutive runs before collecting TORs reported for kinetic parameters. For kinetic experiments on low surface area metal single crystals, the factor most affecting TOR variability is likely to be contamination of the surface by species left after reaction from either the decomposition mechanism itself or transport of external contaminants in the reaction chamber to the crystal surface. These external

ACCEPTED MANUSCRIPT

contaminants may arise from chamber or sample holder contamination, contamination of the reaction gases, or diffusion of contaminants from the bulk of the single crystal to the surface.

Contamination was monitored before and after experiments using XPS and/or AES. Prior to reaction, C and O were already present on the Pt surfaces. Transfer to the reactor introduced both C and O on the surface of the single crystal. Due to poor control of C and O contamination before a reaction, TORs collected on a surface initially completely C- and O-free (according to AES) were not reproducible. Nominal C and O coverages increased on all catalysts after the first ~30 minutes of reaction following cleaning, and then remained constant for subsequent reactions. From XPS, stabilized coverages of C and O ranged between 1-3 ML and 0.4-0.6 ML, respectively, on Pt(111) and Pt(100) surfaces. Typical C and O coverages during several consecutive reactions are plotted in Figure 1.

ACCEPTED MANUSCRIPT

ACCEPTED MANUSCRIPT

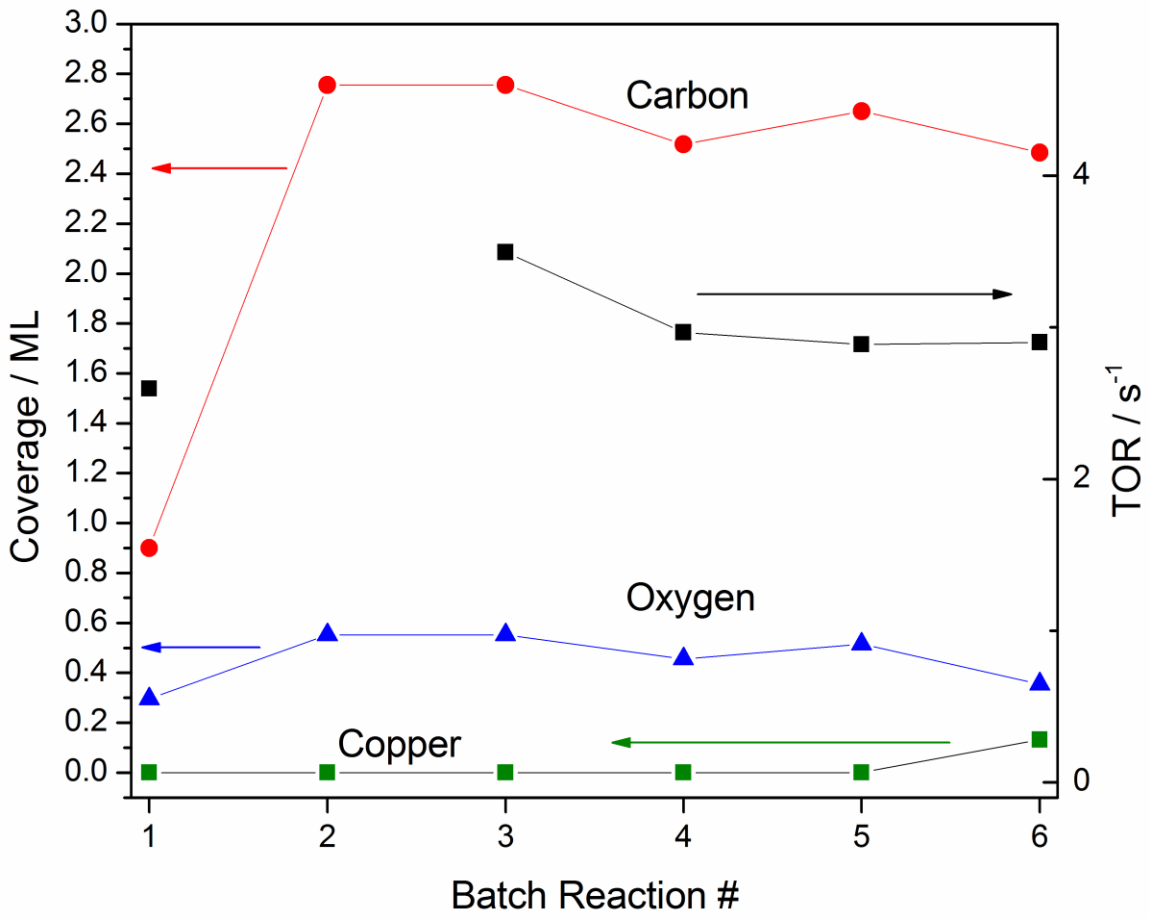

Figure 1. Carbon (red circles), oxygen (blue triangles), and copper (green squares) contaminant coverages calculated from XPS plotted against batch reaction number for a series of consecutive reactions on Pt(111). Also plotted on the right y-axis is the CO_2 TOR (black squares). Reaction conditions were 5 Torr HCOOH, 15 Torr H_2, 15 Torr CO, 800 Torr total (balance N_2), T = 493 K.

ACCEPTED MANUSCRIPT

Other contaminants detected after some reactions were Cu and S. Cu, most likely originating from spot welding with Cu electrodes, migrates from the sides of the single crystal to the front face after several reactions in sequence, since the amount of Cu present after several runs qualitatively tracked with the number of times a single crystal had been spot welded to the sample holder. Above the limit of detection for both AES and XPS, Cu does not affect the TOR more than the run-to-run variability of the rate. From XPS, Cu coverage did not exceed 0.2 ML. However, it should be noted that if the Cu were affecting the rate, it might not need to migrate to the front side of the crystal. In fact, trace Cu was detected on the stainless steel blank sample, which may explain at least some of the background activity of this sample.

S contamination was sometimes observed by AES, but was detected by XPS only once after a reaction with contaminated water. From the high resolution XPS region scan following this reactions, the S coverage was approximately 0.2 ML. From this core level spectrum, the limit of detection was calculated to be approximately 0.07 ML using standard procedures of error calculation in the CasaXPS software. S coverage estimation for small amounts of sulfur is difficult from AES alone due to overlap of Pt NNN and S LMM peaks at a kinetic energy of ca. 150 eV, so from this method typical S contamination coverages were estimated to be $\leq$ 0.07 ML for all runs.

In general, the TOR qualitatively tracks most closely to the coverages of carbon and oxygen. For runs occurring within the first ~30 minutes of cleaning, the rate is usually higher than for subsequent runs for which carbon and oxygen coverages have stabilized. The TOR decreases by about 2 times between the first run and subsequent runs when the rate has stabilized (see Figure 2). This type of deactivation is not unprecedented in this system [4]. Uncorrected peak-to-peak intensity ratios from AES support this assertion. In Figure 2, TORs are plotted for several

ACCEPTED MANUSCRIPT

consecutive batch reactions on Pt(100), and AES peak intensity ratios for the labeled points are given in Table 1. Qualitatively, the rate does not track with S or Cu for the points labeled, as the difference in S_{152}/Pt_{168} and Cu_{920}/Pt_{168} intensity ratios are large before and in a few runs after cleaning, yet the rate is nearly the same.

ACCEPTED MANUSCRIPT

ACCEPTED MANUSCRIPT

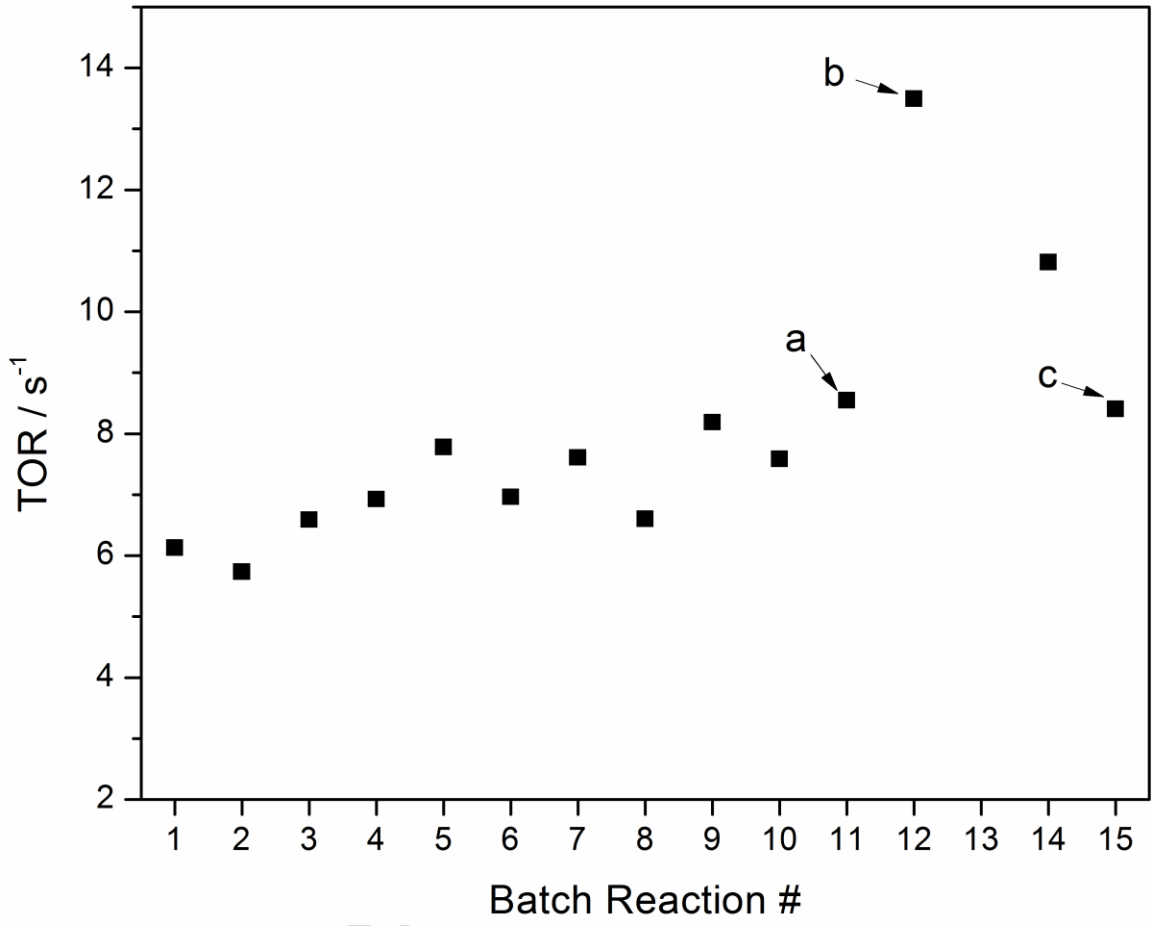

Figure 2. CO_2 TOR for a series of consecutive batch reactions on Pt(100). The point labeled (a) was the 11th batch reaction in series. The sample was cleaned by Ar^+ sputtering and annealing at 1073 K at the point labeled (b). 3 reactions after cleaning, the TOR of the sample returns to the baseline (point (c)). Reaction conditions were 5 Torr HCOOH, 15 Torr H_2, 15 Torr CO, 800 Torr total (balance N_2), T = 503 K.

ACCEPTED MANUSCRIPT

Table 1. Uncorrected AES peak intensity ratios from spectra correspsonding to the labelled points in Figure 2.

Point	C_{272}/Pt_{168}	O_{510}/Pt_{168}	S_{152}/Pt_{168}	Cu_{920}/Pt_{168}
a	2.3	0.6	3.5	0.4
b	0.1	0.1	0.0	0.0
c	2.1	0.5	1.3	0.1

Within a run, the initial rate was stable as evidenced by a plot of CO_2 concentration versus time (shown in Figure S3 in the supporting information). Numerically differentiating the data and converting to a TOR yields a slope standard error that is approximately 3 orders of magnitude smaller than the TOR, a typical slope standard error for a plot of CO_2 concentration versus time within a run. This error, usually on the order of 0.005 s^{-1}, is negligible compared to the day-to-day and run-to-run variability in TOR (± 0.6 and ± 1.0 s^{-1} for Pt(111) and Pt(100), respectively).

Conversion of formic acid was kept below 10%, usually between 1-5%, for each run to ensure that the change in concentration of each gas phase species is much smaller than that species' total concentration.

Kinetics

As discussed above, turnover rates (TORs) for Pt(111) and Pt(100) are normalized to the calculated number of Pt atoms on ideal Pt(111) and (100)-(1x1) surfaces, equal to 1.5 x 10^{15} and 1.3 x 10^{15} atoms cm^{-2}, respectively. Normalized TORs, apparent activation energies, and reaction orders for experiments carried out at standard conditions (5 Torr FA, 15 Torr H_2, 15 Torr CO, 800 Torr total, balance N_2, T = 493 K) are summarized in Table 2. The error in TOR on all

ACCEPTED MANUSCRIPT

catalysts was large on a day-to-day basis: average TORs for Pt(111) and Pt(100) were 2.6 ± 0.6 and 3.7 ± 1.0 molecules CO_2 Pt atom^{-1} s^{-1}, respectively. The areal rate on Pt foil was measured to be (7.5 ± 5.0) x 10^{-9} moles CO_2 cm^{-2} s^{-1}, compared to (6.4 ± 1.5) x 10^{-9} and (8.1 ± 2.2) x 10^{-9} for Pt(111) and (100), respectively.

Table 2. Kinetic parameters for formic acid decompositon at standard reaction condtions (5 Torr HCOOH, 15 Torr H_2, 15 Torr CO, 800 Torr total, balance N_2, T = 493 K). * The TOR on Pt foil assumes an atomic surface density of 1.5x10^{15} atoms cm^{-2}.

			Reaction Orders				
Catalyst	TOR at 493 K/ s^{-1}	E_{app} / kJ mol^{-1}	HCOOH	CO	H_2	H_2O	CO_2
Pt(111)	2.6 ± 0.6	102 ± 14	0.43 ± 0.03	-0.40 ± 0.03	~0	~0	~0
Pt(100)	3.7 ± 1.0	86 ± 11	0.35 ± 0.10	-0.35 ± 0.03	~0	~0	-
Pt Foil	3 ± 2*	94 ± 12	0.35 ± 0.15	-0.43 ± 0.05	~0	-	-

ACCEPTED MANUSCRIPT

Table 3. Kinetic parameters for formic acid decomposition with low initial CO concentrations. Standard conditions were 5 Torr HCOOH, 2-15 Torr H_2, 2 Torr CO, 800 Torr total (balance N_2), T= 463 K. * Error is the standard error of the slope for a single order experiment.

Catalyst	TOR at 463 K/ s^{-1}	E_{app} / kJ mol^{-1}	HCOOH Order	CO Order	H_2 Order
Pt(111)	2.3 ± 0.8	67 ± 11	0.55 ± 0.9*	~0	~0
Pt(100)	2.4 ± 1.0	65 ± 7	(not collected)	~0	~0

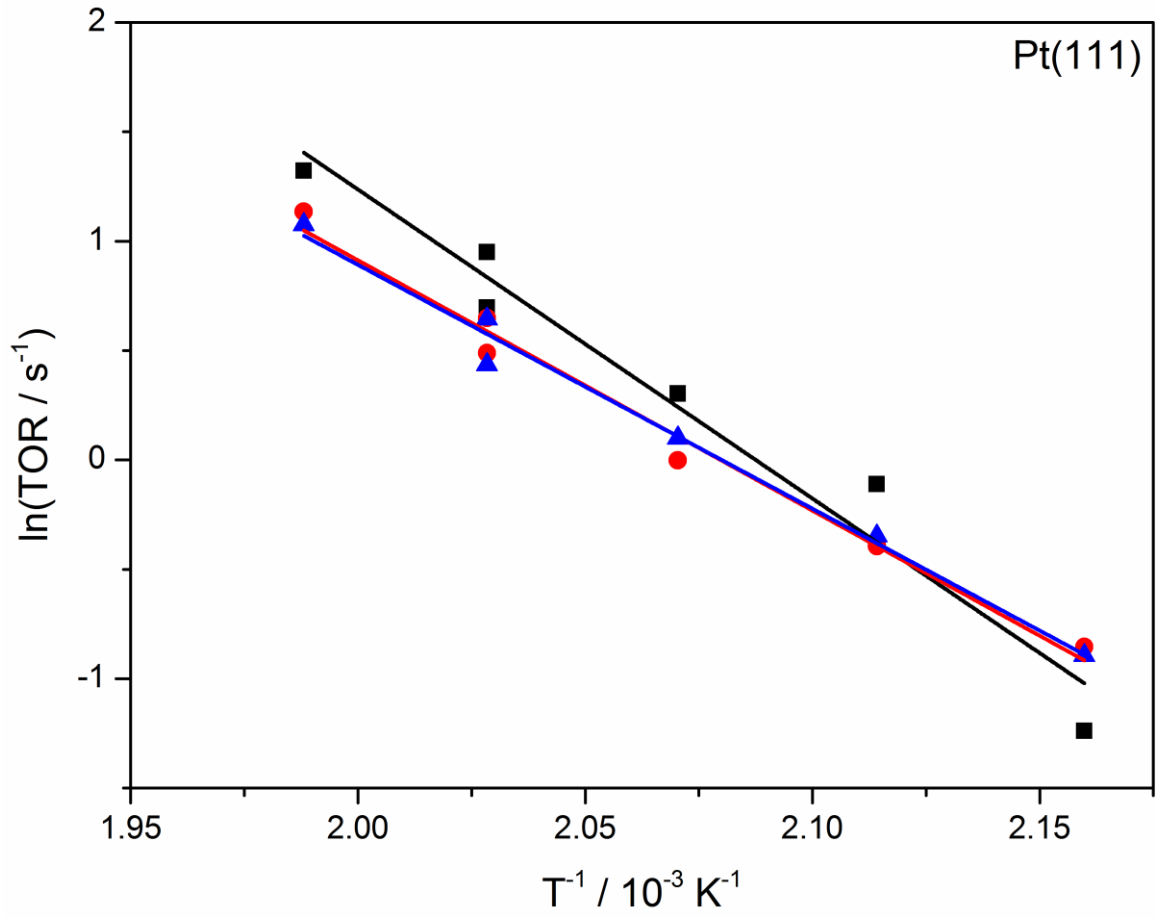

ACCEPTED MANUSCRIPT

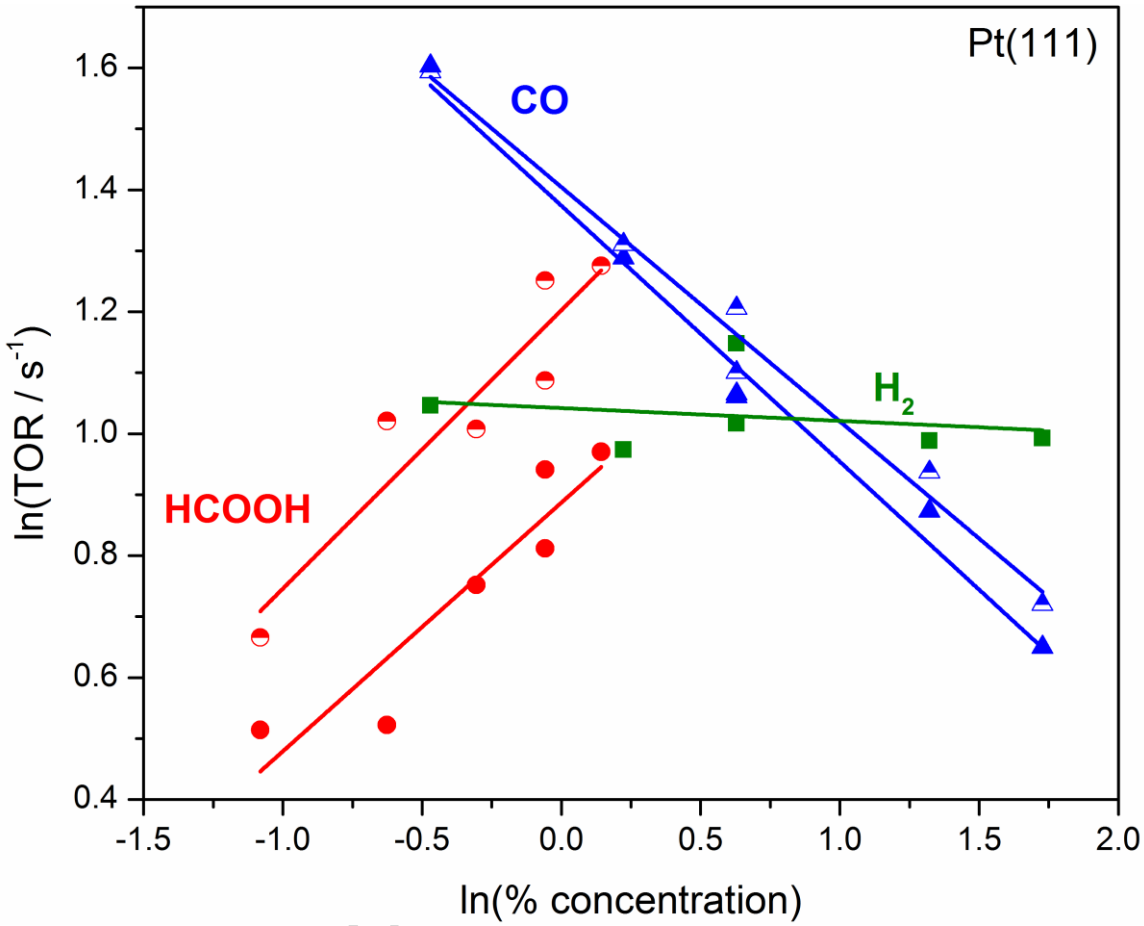

Figure 3. Top: Arrhenius plots for formic acid decomposition on Pt(111). Conditions: 5 Torr HCOOH, 15 Torr H_2, 15 Torr CO, 800 Torr total (balance N_2). Each data series represented by a different shape (square, circle, triangle) represents a different activation energy experiment. Bottom: HCOOH, CO, and H_2 reaction order plots on Pt(111) at T = 493 K. The two sets of data given for HCOOH and CO represent different experiments on different days.

Average apparent activation energies, E_{app}, at standard conditions were 86 ± 11, 102 ± 14, and 94 ± 12 kJ mol^{-1} for Pt(100), (111), and foil, respectively, where the error is one standard deviation of E_{app} values calculated between runs. Runs used to calculate the average values of E_{app} at

ACCEPTED MANUSCRIPT

standard conditions are shown in Figure 3 for Pt(111) to illustrate the data quality, and in Figure S4 in the supporting information for Pt(100).

The average formic acid reaction orders were 0.35 ± 0.10, 0.43 ± 0.03, and 0.35 ± 0.15 for Pt(100), Pt(111), and Pt foil, respectively. These orders are reported with respect to the effective formic acid monomer concentration, which, as discussed earlier, is calculated by addition of the monomer concentration predicted by Equation 1 to two times the dimer concentration predicted by Equation 1. Errors reported for reaction orders represent one standard deviation between runs. Measured CO orders were -0.35 ± 0.03, -0.40 ± 0.03, and -0.43 ± 0.05 on the same surfaces, and H_2 was approximately zero order on all surfaces. H_2O was found to be zero order on Pt(100) and Pt(111), and CO_2 was zero order on Pt(100) using initial CO_2 concentrations less than 200 ppm. Typical reaction order plots for HCOOH, CO, and H_2 on Pt(111) are given in Figure 3 to illustrate data quality and given in Figure S5 for Pt(100) in the supporting information.

Experiments to measure kinetics were also performed on Pt(111) and Pt(100) using lower initial CO partial pressures (standard pressure of 2 Torr). Kinetic parameters at these reaction conditions are summarized in Table 3. Average apparent activation energies on Pt(111) and Pt(100) at these conditions, plotted in Figures S6 and S7, respectively, were 67 ± 11 and 65 ± 7 kJ mol^{-1}, respectively. Under these conditions, the CO reaction order was approximately 0, as shown in Figure S8.

Characterization with XPS

UHV-XPS was used in an attempt to identify surface species left after a reaction and to check the oxidation state of the Pt substrate. The spectra showed that only C and O species were left after a reaction, in addition to the Cu and S contaminants described above. The Pt $4f_{7/2}$ line had a

ACCEPTED MANUSCRIPT

BE of 70.9 eV before and after reaction and was assigned to metallic Pt [12], indicating that the Pt oxidation state was unchanged during reaction. In the C 1s region, it was not possible to differentiate C from formic acid contamination in the background and C left from the reaction. On all surfaces, a peak at about 284.3 eV was observed before and after reaction, assigned to isolated C, chain carbon, or graphitic carbon, which have been reported to produce C 1s BEs of 283.8, 284.1, and 284.8 eV, respectively [13]. After some runs, another peak at around 286 eV was observed, but it was unclear if this peak, assigned to CO-containing species, was left from a true reaction intermediate or re-adsorption of residual gases during transfer of the single crystal. Other than observing accumulation of C and O during the first reaction after cleaning, XPS did not provide additional clues regarding the formic acid decomposition pathway.

DISCUSSION

Measured apparent activation energies for FA:CO concentration ratios < 1 (CO partial pressure = 15 Torr) on the Pt surfaces tested range from 86 ± 11 kJ mol^{-1} for Pt(100) to 102 ± 14 kJ mol^{-1} on Pt(111), with Pt foil having an intermediate activation energy of 94 ± 12 kJ mol^{-1} under the standard conditions used in this study. In all cases, these activation energies are higher than those reported in the literature for other kinetic studies on Pt-containing catalysts for formic acid decomposition. Reported values range between 41-72 kJ mol^{-1} [1, 2, 14, 15]. However, when the initial CO partial pressure was decreased to 2 Torr from 15 Torr, the measured apparent activation energies on Pt(111) and Pt(100) dropped to 67 ± 11 and 65 ± 7 kJ mol^{-1}, respectively, which fall within the range of reported literature values. Furthermore, fractional positive formic acid order values measured in this study are in agreement with a fractional positive order reported for formic acid partial pressures of less than ~15 Torr on Pt/Al_2O_3 [1].

ACCEPTED MANUSCRIPT

Direct comparison of TORs measured in this study to those published for supported Pt catalysts is not possible due to differences in reaction conditions. Nevertheless, some comparisons can be made. Ojeda et al. found that for Pt/Al_2O_3, the TOR decreases with increasing particle size. The turnover rate at their largest particle size, 8 nm, is approximately 1.2 x 10^{-2} molecules HCOOH decomposed per surface metal atom per second at 353 K (30 Torr HCOOH). Extrapolating to 463 K using their measured E_{app} of 72 kJ mol^{-1} measured over the range ~343--383 K yields a TOR of 4.1 s^{-1}. Extrapolating the TOR measured by Solymosi at 423 K on Pt/C to 463 K yields a TOR of 2.1 s^{-1} using their reported E_{app} of 70.7 kJ mol^{-1}, measured in the range 380—425 K in ~38—46 Torr formic acid. For comparison, the average TORs on Pt(111) and Pt(100) for 2 Torr initial CO partial pressure in 800 Torr total pressure at 463 K are 2.3 ± 0.8 and 2.4 ± 1.0 s^{-1}, respectively, but these TORs were collected in the fractional formic acid order regime whereas the studies above measured kinetics in the zero order regime. Extrapolation to the zero-order regime was not performed.

The goal of this work is not to present a comprehensive review of possible mechanistic routes for formic acid decomposition on Pt. In particular, the amount of Pt available under reaction conditions was not measured. The high amount of carbon measured after reaction (1-3 ML) implies the presence of carbonaceous structures in three dimensions. Nevertheless, simple mechanisms were examined to determine the consistency of our data and that in the literature with reasonable assumptions regarding the kinetics of the reaction. Elementary steps include dissociative adsorption of formic acid as formate (HCOO·*; * = site) and a hydrogen atom (H·*), as observed in UHV experiments on Pt(111) [16, 17] and Pt(110) [18], formate dissociation to gaseous CO_2 and another bound hydrogen atom, and finally hydrogen recombination. The literature supports this mechanism by showing that C-H cleavage of the formate hydrogen is

ACCEPTED MANUSCRIPT

kinetically relevant and hydrogen recombination is semi-equilibrated on Pt/Al_2O_3 [1]. A CO adsorption-desorption step was also added. The elementary steps for a single-site formate dissociation step are shown in Equations 3-6:

$$HCOOH + 2* \overset{K_1}{\leftrightarrow} HCOO* + H* \tag{3}$$

$$HCOO* \overset{k_2}{\rightarrow} CO_2 + H* \tag{4}$$

$$2H* \overset{K_3}{\leftrightarrow} H_2 + 2* \tag{5}$$

$$CO + * \overset{K_4}{\leftrightarrow} CO* \tag{6}$$

This mechanism yields the rate equation found in Equation 7, and its derivation can be found in the supporting information:

$$rate = \frac{LK_1k_2K_3^{1/2}[HCOOH]}{[H_2]^{1/2}\left(1 + \frac{K_1K_3^{1/2}[HCOOH]}{[H_2]^{1/2}} + \frac{[H_2]^{1/2}}{K_3^{1/2}} + K_4[CO]\right)} \tag{7}$$

Where *L* is the total number of sites.

This mechanism explains the various reaction order regimes. First, the fractional to zero-order regime transition for formic acid is satisfied, as this mechanism predicts that the formic acid order, n_{HCOOH}, is a function of formate coverage ($n_{HCOOH} = 1 - \theta_{HCOO}$), assuming that higher formate coverages are present at higher formic acid gas phase concentrations. Second, it requires CO order, n_{CO}, to be negative and that $\theta_{CO} = |n_{CO}|$. Finally, the H_2 order (n_{H2}) must be fractional

ACCEPTED MANUSCRIPT

negative. While the hydrogen coverage was not conclusively observed in our experiments, it was found to be close to zero, with the slope of the hydrogen order plots being generally negative but with large standard errors (error = approximately ± 100-200% of the slope). Given that the greatest possible value of n_{H2} is -0.2 at $\theta_{H2} = 0$, we cannot rule out a fractional negative H_2 order from our experiments. Based on the measured formic acid and CO orders, this mechanism predicts steady state coverages of the two species equal to 0.6 and 0.4 ML, respectively.

A similar mechanism includes an extra site in the second elementary step for formate dissocation, with all other steps the same:

$$HCOO* + * \xrightarrow{k_2} CO_2 + H* + * \tag{8}$$

This mechanism yields the rate equation in Equation 9. Its derivation can be found in the supporting information.

$$rate = \frac{zLK_1k_2K_3^{1/2}[HCOOH]}{[H_2]^{1/2}\left(1 + \frac{K_1K_3^{1/2}[HCOOH]}{[H_2]^{1/2}} + \frac{[H_2]^{1/2}}{K_3^{1/2}} + K_4[CO]\right)^2} \tag{9}$$

Where *z* is the coordination number.

This mechanism also explains the phenomena described above for the single site decomposition mechanism including $n_{H2} = -0.2$ at $\theta_{H2} = 0$. Predicted θ_{HCOO} and θ_{CO} coverages are 0.3 and 0.2 ML, respectively. Since the total coverage of surface adsorbates ≥ 0.5 ML in this case, and this range is much less than for the single site mechanism, for which $\theta_{Total} = 1$ (assuming $\theta_{H2} = 0$), the

ACCEPTED MANUSCRIPT

dual site mechanism seems more likely, since the dehydrogenation TOR did not become zero-order in formic acid as the formic acid concentration was increased.

CO was the only possible reaction product observed to affect the rate of reaction and kinetic parameters. A drop in apparent activation energy with lower CO concentrations was observed alongside an increase in the CO order from fractional negative to zero. This behavior is explained at least qualitatively by the Temkin equation [19], which relates the apparent and real activation energies to surface species' reaction orders and enthalpies of adsorption in cases where adsorption equilibrium is reached quickly relative to the rate of surface reaction:

$$E_a = E_{app} - \sum n_i \Delta H_i \qquad (10)$$

Where E_a is the true activation energy, E_{app} is the apparent activation energy, n_i is the reaction order in species i, ΔH_i is the enthalpy of adsorption of species i (negative for exothermic reactions). The enthalpy of adsorption of CO on Pt(111) with a θ_{CO} = 0.4 ML, the calculated CO coverage for HCOOH:CO < 1, is approximately -113 kJ mol^{-1} [20]. In this case, the Temkin equation predicts a real activation energy of about 57 kJ mol^{-1} given the measured apparent value of 102 kJ mol^{-1} and CO order of -0.4. This is within the error of the measured E_{app} in the FA:CO > 1 regime of 67 ± 11 kJ mol^{-1}. On Pt(100)-(1 x 1), using a similar approach and assuming an enthalpy of adsorption of -140 kJ mol^{-1} (measured at 0.5 ML) [21], the Temkin equation predicts a real activation energy of 37 kJ mol^{-1}, lower than the measured value of 65 ± 7 kJ mol^{-1}. In both cases, the calculated activation energy in the fractional negative CO order regime is lower than the measured value in the zero-order CO regime, but this may be the result of the other species present on each surface, which could the CO adsorption energy less exothermic. While the

ACCEPTED MANUSCRIPT

change in order of reaction in formic acid, $n_{HCOOH,}$ from the measured 0.4 here to zero order should also produce a change in apparent activation energy as stated above, the measured value is close to those reported in literature for the zero-order regime. There is no simple, reversible formic acid adsorption step in our proposed mechanisms (i. e., HCOOH + * = HCOOH *). If, instead, the enthalpy of reaction of the first elementary step is used in place of the enthalpy of adsorption of formic acid on Pt(111), calculated to be -38.8 kJ mol^{-1} for a formate coverage of 0.375 and H_2 coverage of 0 ML, respectively [22], then the change in apparent activation energy between the two regimes is expected to be 15.5 kJ mol^{-1}. Given that the absolute value of hydrogen adsorption enthalpy decreases with increasing coverage, this value could be reduced further to about 12.7 kJ mol^{-1} at a hydrogen coverage of 0.4-0.5 ML [23]. Given the error of our experiments and activation energies reported in literature of ~70 kJ mol^{-1}, this is reasonable.

Comparison of the kinetic parameters measured on metal single crystals to those measured on highly dispersed nanoparticles on porous supports is critical, as differences in the parameters may reveal the effect of the catalyst support and/or the effect of small metal particle size. For the case of a catalyst support effect, the reaction may proceed directly on the support or at the interface between the support and active metal. In this study, measured apparent activation energies and reaction orders for runs with low initial CO concentrations are in good agreement with literature values from studies on supported catalysts where CO was not co-fed, supporting the conclusion that the previous supports used with Pt for formic acid decomposition (Al_2O_3 [1], C (Norit) [2]) did not substantially alter the reaction mechanism. In the case of small metal nanoparticles, under-coordinated corner or perimeter atoms on nanoparticles could be responsible for the majority of catalytic activity [24], as has been shown for formic acid decomposition on Au through first principles calculations [25, 26]. Ojeda et al. demonstrated that

ACCEPTED MANUSCRIPT

smaller Pt nanoparticles have a higher TOR than larger nanoparticles [1]. Abbas and Madix, on the other hand, have previously attributed defect sites on Pt(111) to dehydration activity using temperature programmed experiments [27]. Given that selectivity toward dehydrogenation is > 98% [1, 2] (> 99% in this work when CO was not co-fed), consistency with the work of Abbas and Madix would suggest that the smaller Pt nanoparticles used by Ojeda et al. demonstrate superior TORs due to intrinsic electronic effects of smaller nanoparticles, not necessarily because of their most under-coordinated sites (corners, edges). The most under-coordinated sites are likely blocked by CO, either co-fed or produced in the reaction at defect sites but slow to desorb since CO adsorbs more strongly on under-coordinated Pt atoms [28]. At high CO concentrations, CO can also block terrace sites, resulting in the reduction of the dehydrogenation TOR, but at low CO concentrations the effect is negligible, hence the near-zero CO order at CO partial pressures of 2 Torr. In this work, defect sites are also likely to be covered by other contaminants discussed above.

CONCLUSIONS

Formic acid dehydrogenation is not sensitive to the structure of Pt single crystal or foil catalysts tested within the precision of the measurements based on the TORs on Pt(111), Pt(100), and Pt foil at the reaction conditions used. Apparent activation energies for formic acid dehydrogenation measured on Pt(111) and Pt(100) in an initial CO partial pressure of 2 Torr at 800 Torr total pressure around 493 K are in agreement with those obtained from the literature on other Pt catalysts. CO, when included at partial pressures > 2 Torr in the initial reaction gas mixture, was shown to decrease the formic acid TOR on all surfaces, behavior explained qualitatively by the Temkin equation. The results suggest that supports used previously for Pt

ACCEPTED MANUSCRIPT

catalysts (Al_2O_3 [1] and C Norit [2]) do not affect the reaction mechanism, and that under-coordinated sites could be poisoned by CO, which binds strongly to such sites.

ACKNOWLEDGEMENTS

This material is based upon work supported as part of the Institute for Atom-efficient Chemical Transformations (IACT), an Energy Frontier Research Center funded by the U.S. Department of Energy, Office of Science, Office of Basic Energy Sciences.

REFERENCES

[1] M. Ojeda, E. Iglesia, Angewandte Chemie 121 (2009) 4894-4897.
[2] F. Solymosi, Á. Koós, N. Liliom, I. Ugrai, Journal of Catalysis 279 (2011) 213-219.
[3] R. Monteiro, D. Zemlyanov, J. Storey, F. Ribeiro, Journal of Catalysis 199 (2001) 291-301.
[4] A. Smeltz, R. Getman, W. Schneider, F. Ribeiro, Catalysis Today 136 (2008) 84-92.
[5] S. Hagstrom, H.B. Lyon, G.A. Somorjai, Phys Rev Lett 15 (1965) 491-&.
[6] G.R. Schoofs, J.B. Benziger, Surface science 143 (1984) 359-368.
[7] A.S. Coolidge, Journal of the American Chemical Society 50 (1928) 2166-2178.
[8] C.S. Fadley, Electron Spectrosc. Theory, Tech. Appl. 2 (1978) 1-156.
[9] J.H. Scofield, Journal of Electron Spectroscopy and Related Phenomena 8 (1976) 129-137.
[10] J.J. Yeh, I. Lindau, Atomic Data and Nuclear Data Tables 32 (1985) 1-155.
[11] C.J. Powell, A. Jablonski, *NIST Electron Effective-Attenuation-Length Database* - Version 1.3, National Institute of Standards and Technology, in, Gaithersburg, MD, 2011.
[12] J.F. Moulder, J. Chastain, R.C. King, Handbook of X-ray photoelectron spectroscopy: a reference book of standard spectra for identification and interpretation of XPS data, Physical Electronics, Eden Prairie, MN, 1995.
[13] N.M. Rodriguez, P.E. Anderson, A. Wootsch, U. Wild, R. Schlogl, Z. Paal, J. Catal. 197 (2001) 365-377.
[14] W.-J. Chun, K. Tomishige, M. Hamakado, Y. Iwasawa, K. Asakura, J. Chem. Soc., Faraday Trans. 91 (1995) 4161-4170.
[15] J. Block, J. Vogl, Zeitschrift für Elektrochemie, Berichte der Bunsengesellschaft für physikalische Chemie 63 (1959) 3-6.
[16] N.R. Avery, Applications of Surface Science 11 (1982) 774-783.
[17] M. Columbia, A. Crabtree, P. Thiel, Journal of Electroanalytical Chemistry 345 (1993) 93-105.
[18] P. Hofmann, S. Bare, N. Richardson, D. King, Surface Science Letters 133 (1983) L459-L464.
[19] M. Temkin, Acta physicochim. URSS 2 (1935) 313-316.
[20] G. Ertl, M. Neumann, K.M. Streit, Surface Science 64 (1977) 393-410.
[21] P.A. Thiel, R.J. Behm, P.R. Norton, G. Ertl, J Chem Phys 78 (1983) 7448-7458.
[22] T.L. Silbaugh, E.M. Karp, C.T. Campbell, Journal of the American Chemical Society 136 (2014) 3964-3971.
[23] B.J.J. Koeleman, S.T. Dezwart, A.L. Boers, B. Poelsema, L.K. Verhey, Nucl Instrum Methods 218 (1983) 225-229.
[24] W.D. Williams, M. Shekhar, W.-S. Lee, V. Kispersky, W.N. Delgass, F.H. Ribeiro, S.M. Kim, E.A. Stach, J.T. Miller, L.F. Allard, Journal of the American Chemical Society 132 (2010) 14018-14020.

ACCEPTED MANUSCRIPT

[25] S. Singh, S. Li, R. Carrasquillo‐Flores, A.C. Alba‐Rubio, J.A. Dumesic, M. Mavrikakis, AIChE Journal 60 (2014) 1303-1319.
[26] J.A. Herron, J. Scaranto, P. Ferrin, S. Li, M. Mavrikakis, ACS Catalysis 4 (2014) 4434-4445.
[27] N. Abbas, R. Madix, Applications of Surface Science 16 (1983) 424-440.
[28] B. Hammer, O.H. Nielsen, J.K. Norskov, Catal Lett 46 (1997) 31-35.

ACCEPTED MANUSCRIPT

ACCEPTED MANUSCRIPT

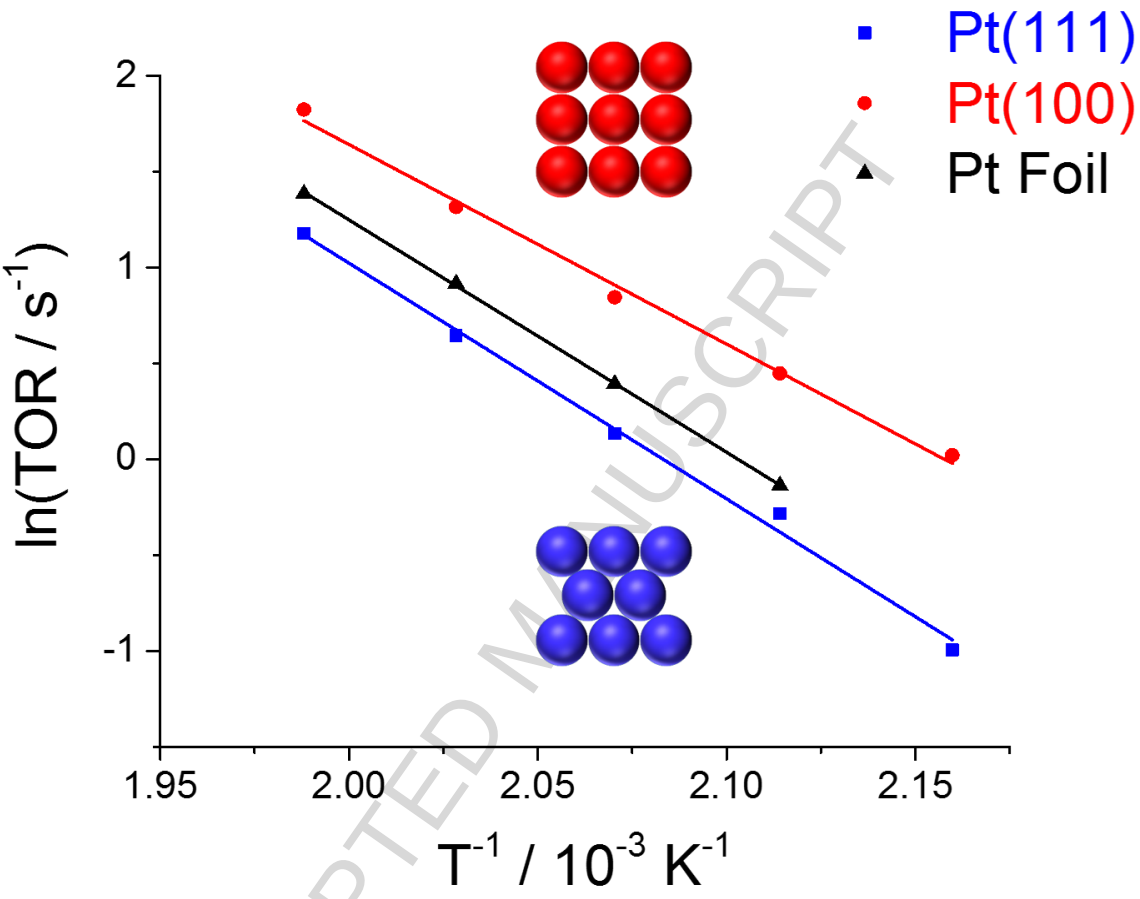

Graphical abstract

ACCEPTED MANUSCRIPT

ACCEPTED MANUSCRIPT

Highlights

- Formic acid dehydrogenation turnover rate not sensitive to Pt surface structure.
- Carbon monoxide depresses dehydrogenation turnover rate on Pt.
- Apparent activation energies qualitatively consistent with Temkin equation.

ACCEPTED MANUSCRIPT